Pergamon

Geochimica et Cosmochimica Acta, Vol. 66, No. 18, pp. 3201–3210, 2002

0016-7037/02 $22.00 + .00

PII S0016-7037(02)00920-1

Dissolution kinetics of magnesite in acidic aqueous solution: A hydrothermal atomic force microscopy study assessing step kinetics and dissolution flux

STEVEN R. HIGGINS,[1,†] GUNTRAM JORDAN[2,*] and CARRICK M. EGGLESTON[1]

[1]Department of Geology and Geophysics, University of Wyoming, Laramie, WY 82071, USA
[2]Institut für Geologie, Mineralogie und Geophysik, Ruhr-Universität, 44780 Bochum, Germany

(*Received June* 26, 2001; *accepted in revised form April* 2, 2002)

Abstract—Magnesite (104) dissolution kinetics were studied in acidic aqueous solutions ($2.0 < pH < 4.2$) at temperatures between 60 and 90°C by atomic force microscopy (AFM). Comparison of dissolution fluxes obtained by AFM and chemical methods revealed six to seven times larger dissolution fluxes obtained by chemical analysis. Corresponding empirical activation energies were found to be 74 ±22 kJ/mol and 41 ± 4 kJ/mol (at pH 4.2) for the AFM and chemical methods, respectively. The empirical reaction order with respect to proton concentration was 0.36 ± 0.13 and 0.47 ± 0.03 for AFM and chemical methods, respectively. These comparisons suggest that the two experimental measurement methods differ as a result of the different sampling length scales associated with the methods. Negligible changes in step dissolution velocity with changes in bulk pH were found, suggesting that the principal source of increasing dissolution flux with decreasing pH is an increase in step density. However, the observed stable step orientation, which is dependent on pH, suggests that more than one proton adsorption equilibrium should be used to describe the surface chemistry of magnesite in acidic solution. *Copyright © 2002 Elsevier Science Ltd*

1. INTRODUCTION

Describing the kinetics of heterogeneous processes occurring at alkaline earth carbonate/water interfaces presents significant challenges for both fundamental and applied research objectives. The dissolution of carbonate minerals may involve multiple heterogeneous reaction mechanisms coupled with homogeneous chemical reactions and mass transport. As a further complication, changes in surface morphology related to defect outcrops can create problems in steady-state approximations on which mechanistic evaluations hinge. Therefore, a descriptive mechanism can be elusive to the most meticulous experimental strategy. Although frustrating for the experimentalist, the implications of these difficulties can create further problems in applied fields whose predictive capabilities can be sensitive to the applicability of heterogeneous mechanisms. The carbonate minerals are important constituents in many environmental processes including carbon cycling and sequestration and biologically mediated mineral formation. These complex environmental systems are regulated by processes that we do not fully understand. Development of a reliable model for the individual reactions that make up a large-scale process can lead to better predictive computational methods in applied fields.

Various models have been proposed for carbonate dissolution in acidic solution (Plummer et al., 1978; Sjöberg and Rickard, 1984a, b; Compton and Unwin, 1990; Van Cappellen et al., 1993; Pokrovsky and Schott, 1999). The overall reaction for calcite dissolution, described by Plummer et al. (1978), is defined by the following reactions:

$$CaCO_3 \overset{k_{H_2O}, k_{-H_2O}}{\longleftrightarrow} Ca^{2+} + CO_3^{2-} \quad (a)$$

$$CaCO_3 + H^+ \overset{k_1}{\longrightarrow} Ca^{2+} + HCO_3^- \quad (b)$$

$$CaCO_3 + H_2CO_3^* \leftrightarrow Ca^{2+} + 2HCO_3^- \quad (c)$$

where $H_2CO_3^* = CO_{2(aq)} + H_2CO_3$. In this parallel reaction scheme, the species are all written in terms of bulk concentrations, and mass transport is assumed to be not important.

Compton and Unwin (1990) showed that under acidic conditions (e.g., at and about pH 3), reaction b was sufficient to describe calcite dissolution kinetics. The Compton and Unwin (1990) work emphasized the importance of relating the flux to the near surface concentration of reactants, and not to that of the bulk fluid, thus demonstrating the significance of fluid transport in the experimental apparatus.

In contrast to calcite, there have been few kinetic studies of magnesite dissolution. At 25°C, Pokrovsky and Schott (1999) report nearly pH-independent dissolution fluxes in the range $0 < pH < 3$ and fluxes proportional to bulk a_{H^+} (a refers to activity) in the range $3 < pH < 5$. The increase of the flux with a_{H^+} in the range $3 < pH < 5$ was attributed to the increasing concentration of $>CO_3H$ surface sites (">" here is used to denote a surface-attached species). Pokrovsky and Schott (1999) used a surface complexation model (SCM) (Pokrovsky et al., 1999) to relate the proton-promoted dissolution flux to the concentration of surface adsorbed protons. Their analysis revealed a fourth-order ($n = 4$) dependence of the dissolution flux on $[>CO_3H]$ (note that $[>CO_3H]$ is not the same as $[H^+]$ *near* the surface), suggesting that the activated surface complex consisted of a hydrated $>Mg^+$ site surrounded by four $>CO_3H$

* Author to whom correspondence should be addressed (shiggins@uwyo.edu).
†*Present address:* Chemistry Department, Wright State University, Dayton, OH 45435.

sites. Chou et al. (1989) reported a linear dependence of the magnesite dissolution flux on a_{H^+} in the range $2 < pH < 5$ at 25°C (i.e., $n = 1$), with no prediction for a weaker ($n < 1$) pH dependence below pH 2.

The microscopic processes that ultimately make up the macroscopic signal obtained in these previous studies may reveal underlying details that could explain the macroscopic observations in a new manner. For example, we do not know if the pH-dependent dissolution flux reported above can be related to an increase in dissolution step velocity or an increase in step density, or both. If protons adsorb at step edges, we could hypothesize that the step velocity should increase with decreasing pH if molecular desorption of the protonated species from the step edge is relatively slow. However, if surface diffusion of unprotonated complexes is slower than detachment of any step edge species, then we need to consider the effects of protonation on the mobile admolecules.

The application of new experimental strategies such as scanning probe microscopy to problems in heterogeneous kinetics at carbonate mineral surfaces has given us new information that cannot be gleaned from homogenized chemical reactor studies on the basis of suspended solid particles in stirred reactors. This information includes thermodynamic quantities such as step free energies and energetic barriers on calcite (Teng et al., 1998), the mechanism by which homovalent impurity cations inhibit calcite growth (Astilleros et al., 2000; Davis et al., 2000), the influence of solution pH on calcite step kinetics (Shiraki et al., 2000), and the influence of orthophosphate on calcite precipitation (Dove and Hochella, 1993). Jordan et al. (2001) examined the step orientation and kink kinetics on magnesite (104) and applied a simple kink dynamic model to describe the observations. They found that diffusion along the surface or step edges may be important to consider in describing the behavior of step edges during magnesite dissolution. In the present study, we have used hydrothermal atomic force microscopy (HAFM) to study the dissolution kinetics of magnesite (104) under conditions similar to those used in Jordan et al. (2001). The purposes of this study are to make comparisons of AFM- and chemically derived dissolution fluxes and to evaluate current macroscopic models for carbonate dissolution in light of the microscopic structural and kinetic observations. Here, we will critically examine our experimental approach and discuss what new information may be obtained from the scanning probe microscopic investigations and how it improves or otherwise changes our visualization of key reaction mechanisms.

2. EXPERIMENTAL METHODS

2.1. Materials

Our magnesite crystals originated in Brumado, Brazil. Electron microprobe analysis showed less than 0.1 mol% Ca and traces of Fe. The amounts of Mn, Cu, and Zn were insignificant (≤0.01 mol%). The aqueous solutions were prepared by adding reagent-grade HCl to 0.1 mol/L KCl in deionized water (resistivity, 18 MΩ cm). The solutions were adjusted to the desired pH at room temperature.

2.2. Methods

For the experiments, we used a continuous-flow hydrothermal atomic force microscope described by Higgins et al. (1998) that enables investigation of the solid/liquid interface at temperatures well above the ambient boiling point of water by pressurization of the flowing fluid. The HAFM was operated in contact mode with uncoated silicon cantilevers (Nanosensors). Effluent solution was collected downstream of the HAFM fluid cell and analyzed with inductively coupled plasma–mass spectrometry (ICP-MS).

The net dissolution flux from the magnesite surface was determined by two independent methods. We assumed that all measurements corresponded to an approximate steady state with respect to the net dissolution flux. The first method utilized ICP-MS (Perkin-Elmer ELAN 6000) analyses for Mg in the cell effluent. With a known fluid flow rate, Q, and an estimate of the geometric sample surface area, A (0.25 ± 0.08 cm^2), on the basis of the crystal dimensions, the concentration of Mg, $[Mg]$, in the effluent is related to the net flux of magnesite into the fluid:

$$J(\text{mol cm}^{-2}\,\text{s}^{-1}) = \frac{[Mg]\cdot Q}{A} \tag{1}$$

Mg concentrations in the effluent ranged from ~10 to 300 ppb with ± 1 to 2% relative uncertainty and a detection limit of ~2 ppb on the basis of variances of blank measurements. Use of Eqn. 1 requires the assumption of a well-mixed reactor (fluid cell). The second analytical method utilized the direct AFM observations to determine the dissolution flux. Here, we used a simple method of counting the number of elementary layers, of height h ($h = 2.7$ Å on magnesite (104)), that had dissolved (over a known period of time) at a fixed location on the surface to yield the layer dissolution frequency, ω. The net dissolution flux is then related to the number of layers dissolved per unit time, ω, by

$$J(\text{mol cm}^{-2}\,\text{s}^{-1}) = \frac{\omega\cdot h}{\Omega}, \tag{2}$$

where Ω is the molar volume of the crystal. An identical approach involves the measurement of step velocity, G (perpendicular to the mean step orientation utilizing a surface landmark as a fixed point of reference), and step density, C, for corresponding steps to give ω:

$$\omega = C\cdot G. \tag{3}$$

Because of the low net dissolution flux of magnesite (relative to microscope drift), we were unable to utilize the change (with time) in the feedback voltage applied to the vertical piezoelectric scanner electrode to determine the dissolution flux (Hong et al., 1997; Jordan et al., 1999).

We found two different types of steps on magnesite during dissolution: straight and rough steps. Straight steps are defined as those that are nominally oriented along the directions $[48\bar{1}]$ and $[\bar{4}41]$, making up the edges of rhombic etch pits. These steps usually appear straight in AFM images, although this is certainly not an appropriate description at the molecular level. Furthermore, these straight steps can be subdivided into "obtuse" and "acute" steps, where these descriptors are commonly used to imply that, in a cross-sectional view, the acute steps "overhang" the lower terrace whereas the obtuse steps form a more open structure with respect to the lower terrace. These steps are sometimes denoted $[48\bar{1}]_o$ and $[\bar{4}41]_o$ for the obtuse steps and $[48\bar{1}]_a$ and $[\bar{4}41]_a$ for the acute steps, or alternatively, $[48\bar{1}]_+$ and $[\bar{4}41]_+$, and $[48\bar{1}]_-$ and $[\bar{4}41]_-$ for the obtuse and acute steps, respectively (Stipp et al., 1994; Paquette and Reeder, 1995). Rough steps are defined as steps that are not oriented along these same directions. A step that is fully roughened would be a step aligned along [010] or $[42\bar{1}]$, where we consider these steps to consist entirely of forced kinks (see Jordan et al., 2001). Previous work on calcite has shown a significant difference, under most experimental conditions, between the velocities of obtuse steps vs. the velocities of acute steps, with obtuse steps commonly retreating two to five times faster than acute steps (Liang and Baer, 1997; Jordan and Rammensee, 1998; Shiraki et al., 2000). We have observed qualitatively similar behavior for the corresponding steps on magnesite, except that the acute steps on magnesite dissolve at least a factor of 50 times slower than the obtuse steps (Jordan et al., 2001). Because the estimated velocity of the acute steps is within the uncertainty of any step velocity measurement made by AFM, here we treat the acute steps as though they are immobile.

To address the influence of mass transport on the experimental

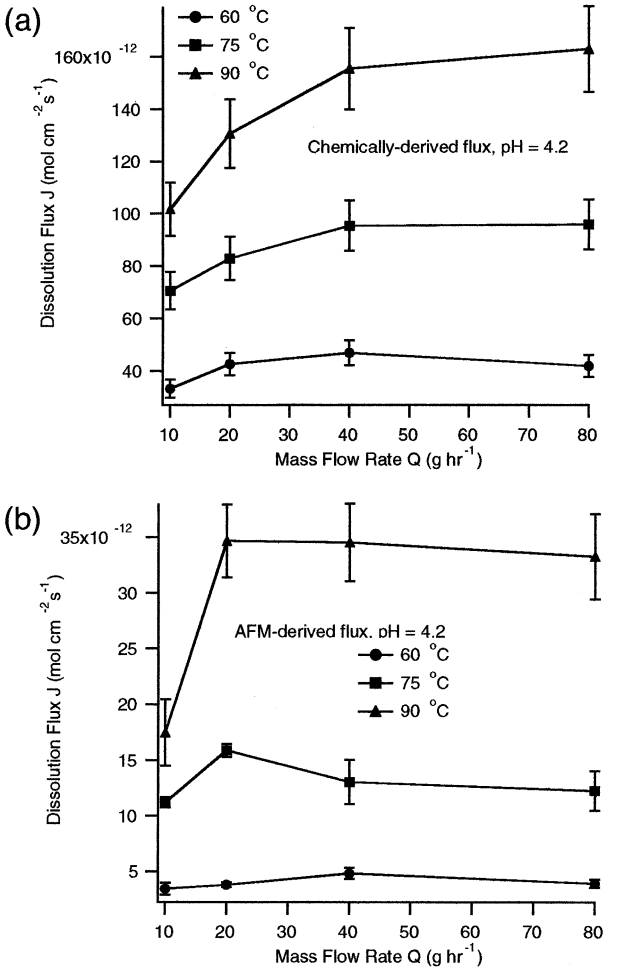

Fig. 1. Experimental dissolution flux of magnesite at pH 4.2 as a function of mass flow rate using (a) data obtained from the fluid cell outlet composition and (b) data obtained from AFM images.

observables (e.g., step velocity, dissolution flux), the fluid flow rate through the HAFM cell was varied by means of a mass flow controller operating downstream of the HAFM fluid cell. This approach is only useful for qualitative discussion and does not permit any definitive conclusions regarding the limiting influence of mass transport in the experiments without further assumptions (Coles et al., 1998).

3. RESULTS

3.1. Flow Rate Dependence

Magnesite dissolves on (104) surfaces in water at pH 4.2 (0.1 mol/L KCl) by retreat of elementary steps similar to the manner by which calcite dissolves at neutral to slightly acidic conditions at room temperature (Jordan and Rammensee, 1998; Shiraki et al., 2000). The flow rate dependence of the dissolution flux is shown in Figure 1 for data determined by both the Mg concentration in the effluent of the fluid cell (Fig. 1a) and by analysis of AFM images (Fig. 1b). A comparison shows that the rates that are based on effluent concentration are six to seven times higher than the AFM derived rates. This is a phenomenon that was observed on calcite by Shiraki et al. (2000) and on other mineral surfaces (e.g., Bosbach, 2002). Although the AFM method should not generally yield results that are comparable to the results based on effluent concentrations, the AFM yields nearly exact rates over the area of examination. The uncertainty in the AFM method is not influenced by scanner calibration, so from an analytical perspective, AFM uncertainty arises from the possibility that sampling is not representative (i.e., by neglecting crystal edges and large cleavage steps). It has been observed that geometric surface areas are usually smaller than those obtained by the Brunauer-Emmett-Teller (Brunauer et al., 1938) adsorption method because the geometric area neglects surface roughness (White and Peterson, 1990). The AFM-based dissolution rate, being normalized to geometric surface area, however, implicitly contains any influence from surface roughness. Although normalizing our chemical rates to the Brunauer-Emmett-Teller area might improve the agreement between data sets, conversely, one could also argue that the AFM-based rate should be higher if regions of higher step density were averaged into the AFM-based rate. The conclusion here should be that neither technique gives the *true* rate (which arguably does not exist), and that the level of detail desired from a given study should dictate which method is *best*. Both data sets show some increase in dissolution flux between 10 g hr^{-1} and 20 g hr^{-1} flow rates, particularly at 90°C. Further increases in mass flow rate generally did not result in significant changes in the dissolution flux determined by either method. Some previous work on calcite growth and dissolution (Liang and Baer, 1997; Shiraki et al., 2000; Teng et al., 2000) has suggested similar findings and the general conclusion in these works is that a lack of change in step and/or surface flux with increase in flow rate signifies a lack of bulk diffusion limitation on flux. This is one interpretation of the data in Figure 1, but a lack of flow rate dependence in the experimental data still requires the assumption that diffusion in the bulk fluid is not important. Only with this assumption is it possible to make quantitative comparisons between different AFM data sets.

3.2. pH Dependence

Figure 2a shows the dissolution flux obtained via both methods vs. bulk pH at T = 60°C. At all experimental pH conditions, the flux determined from the Mg concentration in the cell effluent is significantly higher than that determined from AFM images. The data plotted in Figure 2a were all selected from experimental flow rate regimes in which rates were independent of flow rate within error. The trend in the data indicates a clear increase in the dissolution flux with decreasing bulk pH. This observation is in qualitative agreement with other work on carbonate mineral dissolution in acidic aqueous solution (e.g., Plummer et al., 1978; Chou et al., 1989; Schott et al., 1989; Shiraki et al., 2000) and is consistent with a type of proton-promoted dissolution mechanism. As described for calcite in acidic solutions (e.g., Plummer et al., 1978), the slope of the linear regression of the logarithm of the dissolution flux, *J*, vs. bulk pH can be regarded as the empirical reaction order *n* (with respect to protons) according to

$$J = k_n a_{H^+}^n , \quad (4)$$

where k_n is the rate constant. Use of Eqn. 4 requires several

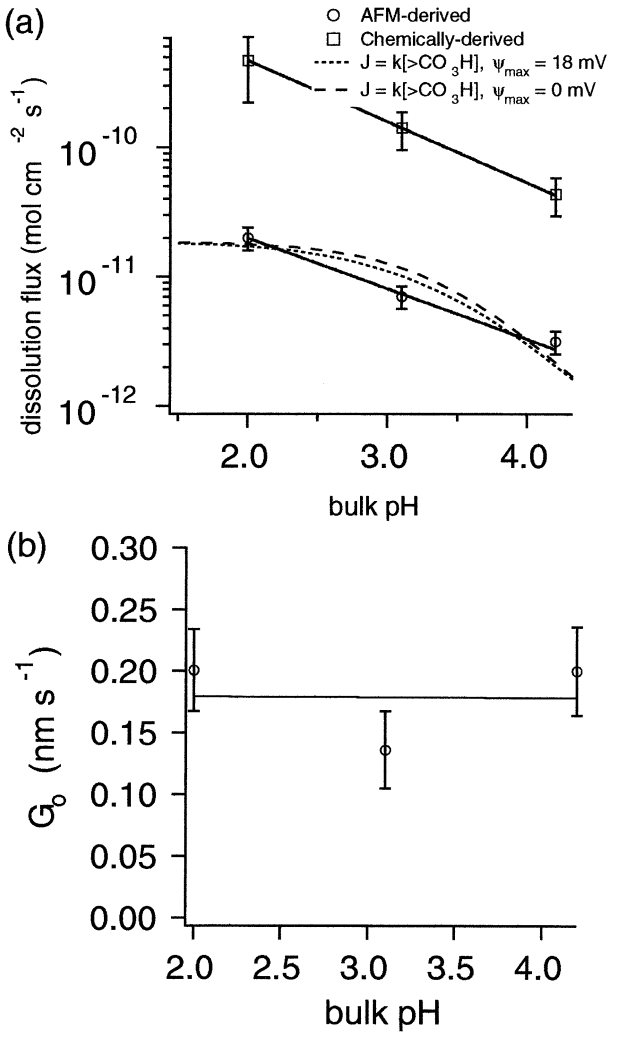

Fig. 2. Experimental (a) dissolution flux and (b) step velocity of magnesite at 60°C as a function of pH in the bulk fluid. Significant discrepancies exist between the flux measured by AFM and the flux measured by the fluid outlet composition. In (a), solid lines are linear least-squares fit lines; dashed lines show the predicted dependence of dissolution flux on pH for a SCM-based mechanism assuming pK_{int} = 3.3, $J = k[>CO_3H]^n$ ($n = 1$), and the maximum surface potential, y_{max}, is 0 mV (long dash) and 18 mV (short dash). Increasing n (i.e., $n = 4$, from Pokrovsky and Schott, 1999), did not improve the agreement between model and data.

assumptions—first, that the simultaneous surface reactions a and c are negligible compared with the contributions from the proton-promoted path (reaction b), where Mg should replace Ca in reactions a to c. The AFM-derived data give $n = 0.364 \pm 0.133$, whereas the analytical chemical data give $n = 0.469 \pm 0.034$. The physical significance of n depends on the identity of the rate-determining step. The relatively weak pH dependence is unexpected on the bases of mechanistic studies showing that a first-order ($n = 1$ in Eqn. 4) proton-promoted mechanism was appropriate for calcite (104) dissolution in acidic solution (Compton and Unwin, 1990). The data may be more consistent with the SCM model of Pokrovsky et al. (1999), which predicts a plateau in the dissolution flux at low pH.

Surprisingly, the velocity, G_o, of steps comprising the obtuse edges of etch pits showed no clear dependence on bulk solution pH (Fig. 2b). The step orientation, however, *is* sensitive to pH (Jordan et al., 2001). As shown in Figure 3, the direction comprising the etch pit perimeter changes as pH is lowered from 4.2 to 2.0. A further observation to be made in comparing Figure 3a with Figure 3b is an increase in the density of monolayer pits (or two-dimensional nuclei) with a decrease in pH. A count of pits in Figures 3a and 3b reveals experimental pit densities of 4 and 9 μm^{-2}, respectively. This is not a tremendous difference unless it is considered that the pit diameters at pH 4.2 tend to be larger than the pit diameters at pH 3.1. Therefore, the finite size of the AFM tip reveals only pits of a certain experimental critical size. For any distribution in pit diameter, the systematic error of pit count will be greater as the distribution mean becomes smaller (i.e., closer to the experimental critical size). This implies that the 9 μm^{-2} pit density measurement in Figure 3b is probably erroneously low. Returning to Eqn. 3 in light of the pH-dependent data, we conclude that the dissolution flux changes primarily with the step density.

3.3. Temperature Dependence

From both sets of temperature-dependent dissolution data, an apparent activation energy for the overall dissolution reaction can be calculated (Fig. 4). The AFM derived activation energy is 74 ± 22 kJ/mol. By use of Mg analysis–based fluxes, the apparent activation energy is 41 ± 4 kJ/mol. Changes in the bulk proton activity with temperature were negligible between 25 and 90°C. The apparent activation energies will contain energetic barriers to adsorption/desorption and surface diffusion, provided that they are significantly larger than kT (k is the Boltzmann constant), and any temperature dependence of equilibrium constants relevant to the formation of the activated complex. A full evaluation of these energies is not possible as a result of multiple unknown energetic quantities, but the fact that the two experimentally derived activation energies differ is significant. We shall examine this discrepancy in further detail in the discussion below.

4. DISCUSSION

4.1. AFM Observations

Given the very low observed magnesite dissolution flux relative to that of calcite (e.g., Chou et al., 1989), it is unlikely that magnesite dissolution is impeded significantly by mass transport in the bulk. Our examination of the flow rate influence on dissolution flux (Fig. 1) revealed, however, that at lower flow rates bulk transport is important to consider and therefore stipulating that transport need not be considered is not justifiable. Because the data in Figures 2 and 4 were taken exclusively from higher flow rate conditions, the proton concentration near the surface is likely to be comparable to that in the bulk solution.

The AFM results in the range $2 < pH < 4.2$ gave an empirical reaction order (Eqn. 4) with respect to $[H^+]$ of ~0.36. Interpreting the physical significance of this reaction order is challenging even at the microscopic level because we do not know the spatial distribution of or the density of surface charge, which would influence the electrostatic contribution to the overall free energy of proton adsorption. With the work of

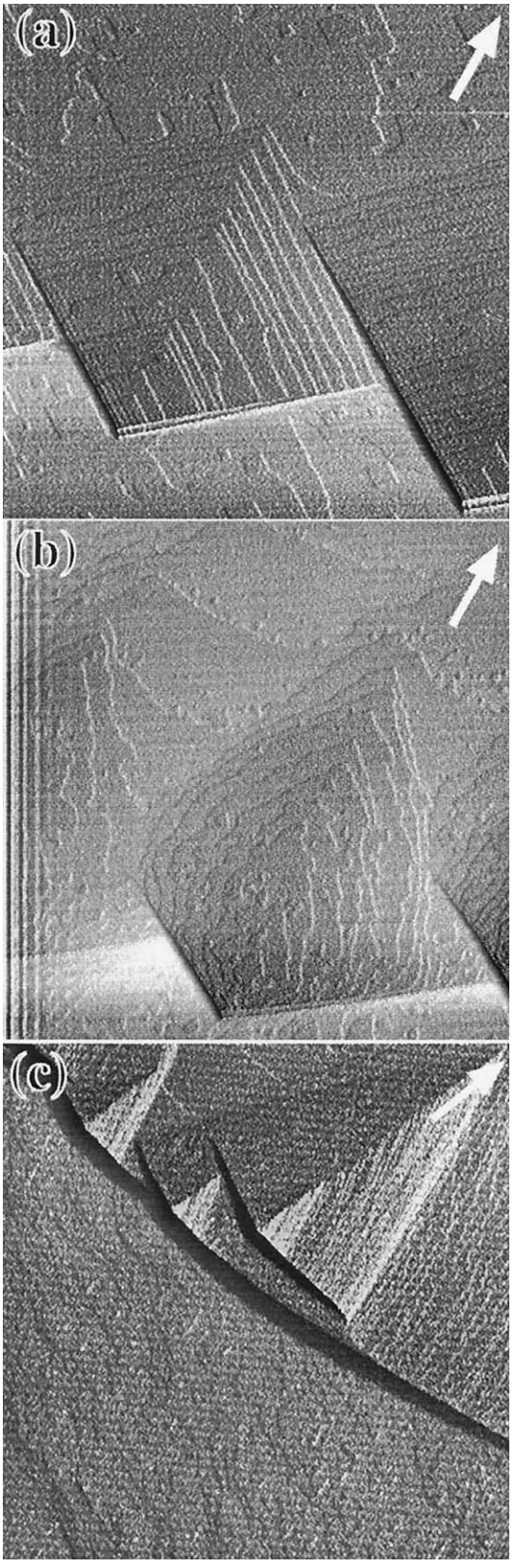

Fig. 3. AFM images (2.5 × 2.5 μm) of the magnesite surface during dissolution at 60°C and (a) pH 4.2, (b) pH 3.1, and (c) pH 2.0 in the bulk. The projection of the c-axis (arrowhead going into the page) is shown in each image.

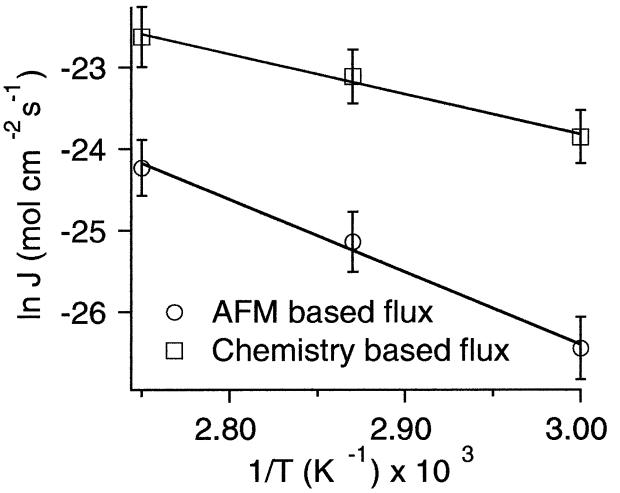

Fig. 4. Plot of ln flux vs. 1/T for magnesite dissolution at pH 4.2. Squares represent the chemically derived dissolution flux and circles represent the AFM-derived flux. Apparent activation energies determined by least-squares fitting were 41 and 74 kJ/mol for the chemical and AFM data, respectively.

Pokrovsky et al. (1999), we can estimate the influence of electrostatics on our experimental observations.

4.1.1. Electrostatic influence on K_a

The effective equilibrium constant $K_{a(eff)}$ for a proton adsorption/desorption equilibrium reaction is expressed as

$$>CO_3H \Leftrightarrow >CO_3^- + H^+ \qquad \text{(e)}$$

$$K_{a(eff)} = K_{a(\text{int})} e^{-\frac{F\psi}{RT}}, \qquad (5)$$

where ψ is the surface potential, $K_{a(int)}$ is the intrinsic chemical equilibrium constant and the other symbols have their usual meaning. To estimate ψ in our experiments, we utilize the maximum calculated value of 54 mV from Pokrovsky et al. (1999) determined at 25°C and 0.01 mol/L ionic strength. The interfacial capacitance should be proportional to the square root of the ionic strength and therefore, the interfacial capacitance in our experiments (0.1 mol/L) should be approximately three times higher. Use of the constant capacitance model charge-potential relationship predicts our maximum surface potential to be ~18 mV resulting in $K_{a(eff)}$ decreasing by only 50% as the pH is brought below $pK_{a(int)}$. The effect of this electrostatic contribution on the proton adsorption isotherm is shown in Fig. 2a. With such a minor influence of electrostatics on the concentration of adsorbed protons, we may conclude that neglecting this effect is justified here. The number of adjustable parameters (involved in calculating surface speciation) compared with the number of data points does not warrant attempting to fit the data with a SCM. Furthermore, in this specific data set, the linear function will always fit the data points better than the SCM unless very large surface potentials (much larger than those reported in Pokrovsky et al., 1999) are allowed. This does not suggest that the SCM is inappropriate, but only that a SCM based on a single proton adsorption reaction (reaction e) in this

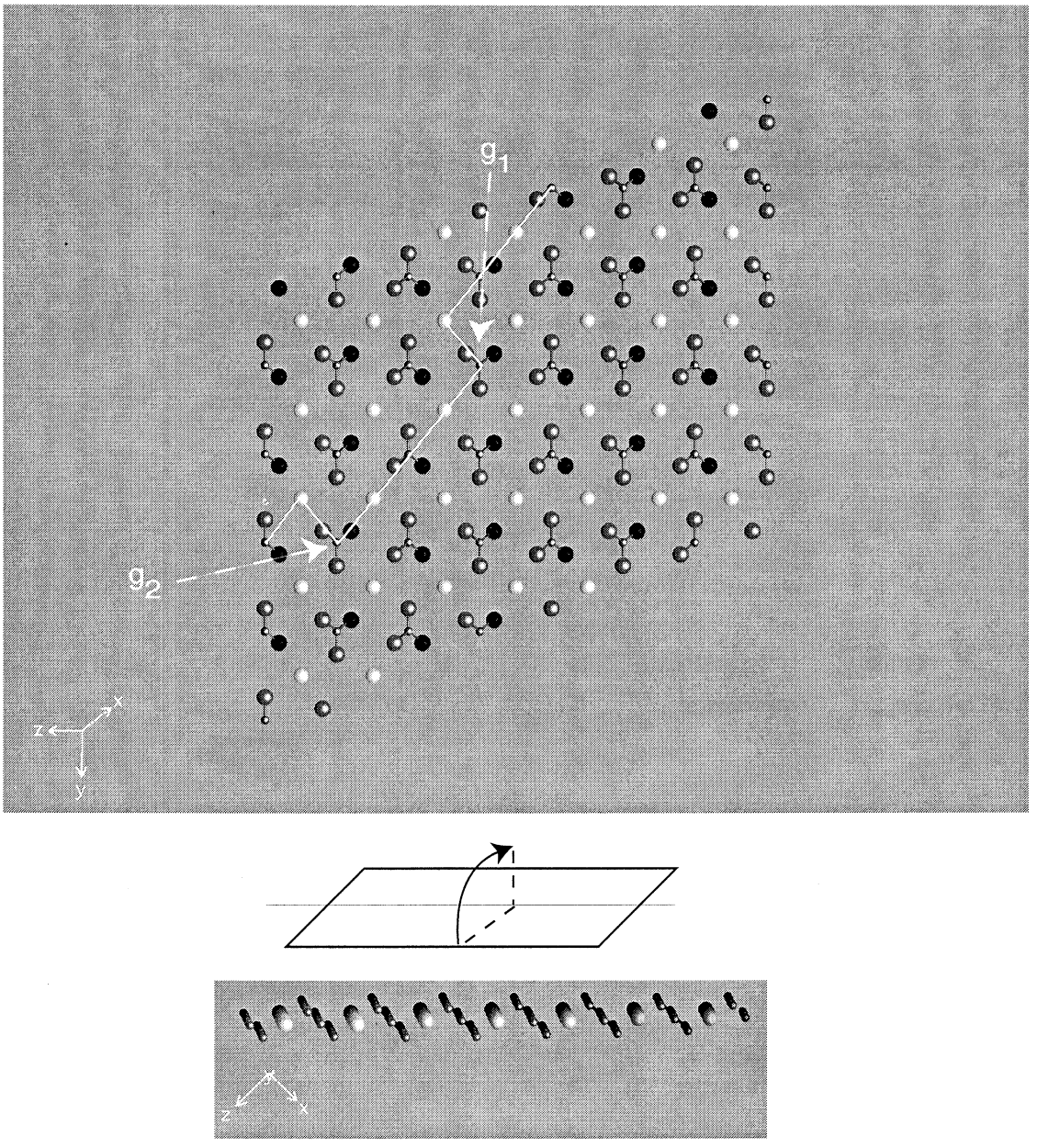

Fig. 5. Atomic structure of the magnesite (104) surface showing a hypothetical step edge with carbonate-terminated kink sites (top). The g_1 site consists of a carbonate group exposed on its molecular plane, whereas at the g_2 site, the edge of the molecular plane is exposed. The line drawing shows the rotation of the top image to generate the bottom image, which in turn illustrates the tilt of the carbonate groups in the surface plane.

pH range may be insufficient. Next, we will consider how the microtopography may further support this possibility.

4.1.2. Existence of more than one proton adsorption reaction

The velocity of steps defining the etch pit shapes was found to be essentially independent of pH in the range $2.0 < \text{pH} < 4.2$, whereas the step orientation was sensitive to the pH conditions. We can think of any one of the straight steps to consist of two different carbonate step sites and four different carbonate kink sites, making six different possible proton adsorption sites on a single type of step. Two kink sites are oriented in a manner in which the carbonate group is exposed on the molecular plane whereas the other two kinks expose the carbonate group essentially on edge. Figure 5 shows the magnesite surface structure to illustrate this point. The kinked line drawn in the top figure denotes the position of a hypothetical obtuse step edge (stepping down from left to right in the figure). The carbonate group at the g_1 kink site is exposed primarily on the molecular plane whereas the carbonate group at the g_2 kink site is exposed at its edge. This scenario is but one of several possible kink terminations for this step because of the alternating orientation of the carbonate groups along the straight step

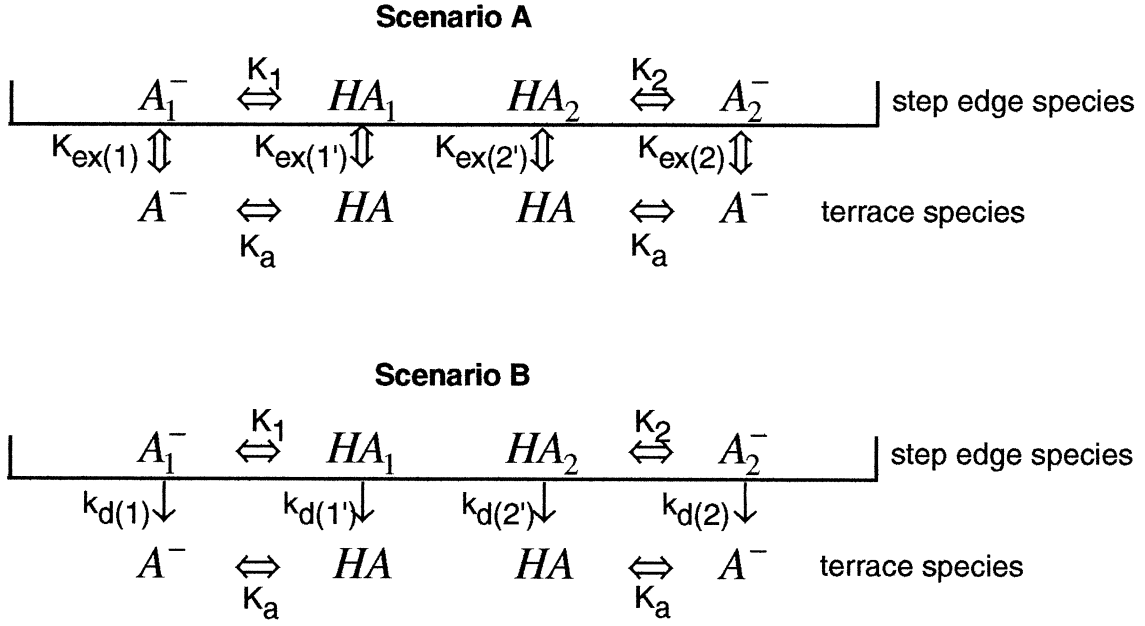

Fig. 6. Reaction scenarios for carbonate (A^-) and bicarbonate (HA) species at and near the step edge. Subscripted species belong to the step edge (i.e., kink sites), whereas nonsubscripted species are the desorbed (i.e., terrace) species adjacent to the step edge. Double arrows indicate reversible, equilibrium reactions. Single arrows indicate irreversible reactions.

directions. It is also possible to describe an equal number of kink sites along the acute steps.

To reduce the level of detail for this discussion, we will simplify the kink termination possibilities so that each step edge has effectively only two carbonate terminations: One termination corresponding to a left-handed kink, and one corresponding to a right-handed kink. For a given pH in equilibrium with respect to proton adsorption (which we will always assume), a higher fraction of one type of site could possess an adsorbed proton. By extension, we also suggest that admolecules or adions existing *on* the terraces will also have an associated pK_a that will be larger than any of the kink or step pK_a*s* on the basis of simple coordination number considerations.

In light of the distinction in protonation sites, we can develop the following step reaction scheme (Fig. 6) to better understand the AFM observations. The four carbonate sites (A_1^-, A_2^-, HA_1, and HA_2) are in equilibrium with the protons in the near-step solution phase, implying the following relationships:

$$K_1 = \frac{A_1^-[H^+_{(kink)}]}{HA_1},$$

$$K_2 = \frac{A_2^-[H^+_{(kink)}]}{HA_2}, \qquad (6)$$

where HA_1, HA_2, A_1^-, and A_2^- are the densities of the corresponding kink sites on the step edge.

A step will not change orientation rapidly in response to a change in pH (which has additional implications discussed below), but will change orientation on a much longer timescale, governed by the kinetics of kink detachment and the length of the step. Two main scenarios we will consider are detailed in Figure 6.

Scenario A is the case where all kink-terrace exchange reactions are reversible (as indicated with double arrows). The rate-determining step then is assumed to be subsequent surface diffusion of the species away from the step edge and onto the terrace or desorption of terraces species into solution. An increase in proton concentration near the surface will shift all acid equilibria toward higher concentrations of protonated species. If $K_1 = K_2$, then the step will not change orientation under the equilibrium assumption. A change in step orientation here, as we have observed, implies that the corresponding changes in free energies of proton adsorption must not be equal (i.e., $\Delta G(HA_1) \neq \Delta G(HA_2)$). The change in step orientation in this scenario must be linked to a minimization in the edge free energy. Therefore, our observations thus far are consistent with $K_1 \neq K_2$ when scenario A is used.

What are the predicted consequences of scenario A on the velocity of an isolated step edge subjected to a decrease in pH? As long as the kink density on the step is constant and determined only by thermal fluctuations, there should be no change in the step velocity. Immediately after the drop in pH, a transient increase in the step velocity should occur because the initial step orientation is not coincident with the new preferred (i.e., slowest) step orientation.

Scenario B considers the possibility that all detachment reactions from the step edge are irreversible (as indicated with single arrows). In this case, the overall rate-determining step is detachment from the step edge. The step orientation will reflect differences in kink detachment frequency ($k_{d(1)} + k_{d(1')}$ vs. $k_{d(2)} + k_{d(2')}$) of the sites and with $K_1 \neq K_2$, this would have to be taken into account in addition to the detachment kinetics. The

two opposing kink detachment processes are manifested in the step orientation that favors the persistence of kinks with slower detachment kinetics (see Jordan et al., 2001). In essence, the increased rate of detachment at one kink site is offset by the decrease in its corresponding density. The net effect is a change in the step orientation. The change in the step velocity will depend on the kink densities, which are not known with certainty at this point. We have presumed that the carbonate sites are slow to detach with the metal site rapidly detaching after this slow step. This presumption could be equivalently replaced with the supposition that detachment of the hydrated metal sites is slow (whether on a carbonate, or other mineral such as an oxide), providing a more direct link between the heterogeneous kinetics and the identity of the metal cation (e.g., Casey, 1991; Pokrovsky and Schott, 2002).

Jordan et al. (2001) discussed kink kinetics on magnesite (104) and suggested that one possible systematic error in the measurements of detachment frequencies resulted from slow surface diffusion, implying that detachment from the step edge is at least partially reversible (i.e., supporting scenario A).

The change in step orientation with pH is strong evidence in support of differing pK_a values associated with different kink sites. These considerations provide explanations for the observed change in step orientation with pH, but the pH-independent step velocity provides little help in explaining the pH-dependent dissolution flux. To explain the fractional reaction order obtained in Figure 2 for the AFM derived fluxes, we turn toward processes that influence the step density (i.e., Eqn. 3).

4.1.3. Step density

It is well known that the net flux in two-dimensional nucleation and growth mechanisms can be described phenomenologically by the following (e.g., Nielsen, 1984; Sangwal, 1987):

$$J \propto h(I_{2D}G^2)^{1/3}, \tag{7}$$

where I_{2D} is the rate of two-dimensional nucleation. The step density, C, is determined by the quotient

$$C = \left(\frac{I_{2D}}{G}\right)^{1/3}. \tag{8}$$

The specific step velocities that are pertinent to Eqns. 7 and 8 are those that limit the rate of etch pit lateral growth, which are the steps defining the shape of the etch pits. Shiraki et al. (2000) reported a rather weak pH dependence to the step velocity on dissolving calcite (104) in near neutral pH solutions with a significant increase in the step velocity at more acidic (e.g., bulk pH 4.4) conditions. The data presented by these authors also showed that, within the fluid flow ranges reported, the step velocity did not reach a limiting value at pH 4.4. It is not known how the step velocity on calcite changes with pH below pH 4.4 because the dissolution flux is significantly limited by proton mass transport over a wide range of fluid flow rates (Compton and Unwin, 1990). Our observations show that G_o is essentially pH independent in this study and therefore, I_{2D} must be primarily responsible for the pH dependence of the dissolution flux. The empirical reaction order obtained from the HAFM-derived fluxes is consistent with a first-order dependence of I_{2D} on $[H^+]$ for an overall reaction order of 1/3 with respect to $[H^+]$ as in Eqn. 7. An increase in the rate of two-dimensional nucleation with increasing $[H^+]$ is further supported by the images shown in Figure 3. It is interesting to point out that at pH 2 (Fig. 3c), we did not observe any two-dimensional nuclei as at pH 3.1 (Fig. 3b). We suggest that the actual rate of two-dimensional nucleation is greater at pH 2 than at pH 3.1, but that two factors give the opposite appearance in the AFM images. First, the higher step density due to a larger I_{2D} in Figure 3c leaves only small terrace areas, defined by perhaps only a few pixels, on which to observe monolayer pits. Second, the higher dissolution flux results in a shorter lifetime for a monolayer pit, thereby reducing the probability for observing a pit with the AFM. An increase in monolayer pit nucleation rate is also predicted on the basis of the relationship between two-dimensional nucleation rates and the thermodynamic driving force for dissolution (i.e., undersaturation) (e.g., Sangwal, 1987).

The above results do not unambiguously show that the AFM-based reaction order must be explained by Eqns. 7 and 8. Given the possibility for numerous proton adsorption equilibria on this surface, a single site SCM clearly oversimplifies the surface reactions. To address these multiple reactions would require further information on the range of adsorption constants that may be expected for various sites and information on the spatial distribution of charge on the surface.

4.2. Comparison of Methods

Although both sets of dissolution data were obtained from the same experiment, the two data sets are not comparable. The differences arise from several factors that we will discuss here. One problem with our study of the macroscopic or bulk dissolution of magnesite lies in our steady state approximation. Because the sample is inherently heterogeneous because of the crystal edges and linear defects, we might also expect the dissolution flux to be heterogeneous (Schott et al., 1989). Therefore, the macroscopic measurements are likely to provide different information than AFM measurements. The dissolution flux will generally be highest at the terminating crystal edges and highly strained defects because there is little or no barrier to generation of new step edges. These regions of high flux will spread laterally, engulfing regions of lower flux on a timescale approximately equal to the distance between defects divided by the step velocity. Beyond this timescale, the crystal would be dissolving at a rate that may be approximated as constant (e.g., MacInnis and Brantley, 1992).

We have made the argument that mass transport is not a limiting factor in our AFM experiments, but this may not hold for regions of higher dissolution flux. It is possible that dissolution at high step density regions near the crystal edges and around macrocleavage steps is limited, at least in part, by bulk diffusion. The experimental activation energies (Fig. 4) further support this in that the factors limiting dissolution on relatively flat surface regions are clearly not the same factors governing macroscopic dissolution.

5. CONCLUSION

The results described above provide a unique illustration of the magnesite/water interface and the associated dissolution

kinetics. Our results showed that AFM and chemical methods for determination of dissolution flux provide different results. This leads us to conclude that the two methods do not account for the same processes because of the different sampling length scales associated with the methods. This conclusion is further supported by empirically determined activation energies of 74 $\pm$22 kJ/mol and 41 $\pm$ 4 kJ/mol (at pH 4.2) and empirical reaction orders with respect to proton concentration of 0.36 $\pm$ 0.13 and 0.47 $\pm$ 0.03 for the AFM and chemical methods, respectively.

We found that the dissolution step velocity does not change significantly with changes in bulk pH, suggesting that the principal cause of increasing dissolution flux with decreasing pH is an increase in step density. The observed stable step orientation, which was dependent on pH, suggests that more than one proton adsorption equilibrium should be used to describe the surface chemistry of magnesite in acidic solution. This has further implications in that models describing the surface chemistry of magnesite in acidic solution with only a single protonation constant may be oversimplified. The lack of step velocity change (but the observed change in step orientation) with solution pH may imply that the magnesite dissolution kinetics is not controlled by detachment at kink sites. On the bases of step observations, surface diffusion, desorption, or both from the surface as the rate controlling mechanistic steps is more likely. We cannot suggest that surface diffusion is relevant to the dissolution flux with more certainty without additional information. Studies of the spatial and temporal step edge fluctuations (Pimpinelli et al., 1993; Bartelt et al., 1994; Girard et al., 1994; Giesen et al., 1996; Yau et al., 2000) should offer additional evidence leading to more definitive conclusions regarding the role of step edges in the dissolution of magnesite.

Acknowledgments—We thank Kevin Knauss (Lawrence Livermore National Laboratory) for helpful discussions, Rolf Hollerbach (Mineralogisches Museum der Universität zu Köln) for kindly providing excellent samples, and Dr. Jacques Schott and two anonymous reviewers for providing very useful suggestions for improving the manuscript. We also thank the Deutsche Forschungsgemeinschaft (Jo 301/1-1,2 to GJ), and the U.S. Department of Energy, Offices of Science and Environmental Management (DE-FG03-96SF14623 to CME and SRH and DE-FG07-99ER15019 to CME) for financial support.

Associate editor: J. Schott

REFERENCES

Astilleros J. M., Pina C. M., Fernández-Díaz L., and Putnis A. (2000) The effect of barium on calcite {10–14} surfaces during growth. *Geochim. Cosmochim. Acta* **64,** 2965–2972.

Bartelt N. C., Einstein T. L., and Williams E. D. (1994) Measuring surface mass diffusion coefficients by observing step fluctuations. *Surf. Sci.* **312,** 411–421.

Bosbach D. (2002) Linking molecular scale barite precipitation mechanisms with macroscopic crystal growth rates. In *Water-Rock Interactions, Ore Deposits, and Environmental Geochemistry: A Tribute to David A. Crerar,* 1 Vol. Special Publications No. 7. (ed. R. Hellmann and S. A. Wood), pp. 97–110. The Geochemical Society.

Brunauer S., Emmett P. H., and Teller E. (1938) Adsorption of gases in multimolecular layers. *J. Am. Chem. Soc.* **60,** 309–319.

Casey W. H. (1991) On the relative dissolution rates of some oxide and orthosilicate minerals. *J. Colloid Interface Sci.* **146,** 586–589.

Chou L., Garrels R. M., and Wollast R. (1989) Comparative study of the kinetics and mechanisms of dissolution of carbonate minerals. *Chem. Geol.* **78,** 269–282.

Coles B. A., Compton R. G., Suárez M., Booth J., Hong Q., and Sanders G. H. W. (1998) A hydrodynamic atomic force microscopy flow cell for the quantitative measurement of interfacial kinetics: The aqueous dissolution of salicylic acid and calcium carbonate. *Langmuir* **14,** 218–225.

Compton R. G. and Unwin P. R. (1990) The dissolution of calcite in aqueous solution at pH $<$ 4: Kinetics and mechanism. *Phil. Trans. R. Soc. Lond. A* **330,** 1–45.

Davis K. J., Dove P. M., and DeYoreo J. J. (2000) The role of Mg^{2+} as an impurity in calcite growth. *Science* **290,** 1134–1137.

Dove P. M. and Hochella M. F. (1993) Calcite precipitation mechanisms and inhibition by orthophosphate: In situ observations by scanning force microscopy. *Geochim. Cosmochim. Acta* **57,** 705–714.

Giesen M., Icking-Konert G. S., Stapel D., and Ibach H. (1996) Step fluctuations on Pt(111) surfaces. *Surf. Sci.* **366,** 229–238.

Girard J. C., Gauthier S., Rousset S., Sacks W., deCheveigné S., and Klein J. (1994) Dynamics of high index step equilibrium fluctuations as observed by scanning tunneling microscopy. *Surf. Sci.* **301,** 245–252.

Higgins S. R., Eggleston C. M., Knauss K. G., and Boro C. O. (1998) A hydrothermal atomic force microscope for imaging in aqueous solution up to 150°C. *Rev. Sci. Instrum.* **69,** 2994–2998.

Hong Q., Suárez M. F., Coles B. A., and Compton R. G. (1997) Mechanism of solid/liquid interfacial reactions: The maleic acid driven dissolution of calcite—An atomic force microscopy study under defined hydrodynamic conditions. *J. Phys. Chem. B* **101,** 5557–5564.

Jordan G. and Rammensee W. (1998) Dissolution rates of calcite-(1014) obtained by scanning force microscopy: Microtopography-based dissolution kinetics on surfaces with anisotropic step velocities. *Geochim. Cosmochim. Acta* **62,** 941–947.

Jordan G., Higgins S. R., and Eggleston C. M. (1999) Dissolution of the periclase(001) surface: A scanning force microscope study. *Am. Mineral.* **84,** 144–151.

Jordan G., Higgins S. R., Eggleston C. M., Knauss K. G., and Schmahl W. W. (2001) Dissolution kinetics of magnesite in acidic aqueous solution, a hydrothermal atomic force microscopy (HAFM) study: Step orientation and kink dynamics. *Geochim. Cosmochim. Acta* **65,** 4257–4266.

Liang Y. and Baer D. R. (1997) Anisotropic dissolution at the $CaCO_3$(1014)-water interface. *Surf. Sci.* **373,** 275–287.

MacInnis I. N. and Brantley S. L. (1992) The role of dislocations and surface morphology in calcite dissolution. *Geochim. Cosmochim. Acta* **56,** 1113–1126.

Nielsen A. E. (1984) Electrolyte crystal growth mechanisms. *J. Cryst. Growth.* **67,** 289–310.

Paquette J. and Reeder R. J. (1995) Relationship between surface structure, growth mechanism, and trace element incorporation in calcite. *Geochim. Cosmochim. Acta* **59,** 735–749.

Pimpinelli A., Villain J., Wolf D. E., Métois J. J., Heyraud J. C., Elkinani I., and Uimin G. (1993) Equilibrium step dynamics on vicinal surfaces. *Surf. Sci.* **295,** 143–153.

Plummer L. N., Wigley T. M. L., and Parkhurst D. L. (1978) The kinetics of calcite dissolution in CO_2-water systems at 5° to 60°C and 0.0 to 1.0 atm CO_2. *Am. J. Sci.* **278,** 179–216.

Pokrovsky O. S. and Schott J. (1999) Processes at the magnesium-bearing carbonate/solution interface: II. Kinetics and mechanism of magnesite dissolution. *Geochim. Cosmochim. Acta* **63,** 881–897.

Pokrovsky O. S., Schott J., and Thomas F. (1999) Processes at the magnesium-bearing carbonates/solution interface: I. A surface speciation model for magnesite. *Geochim. Cosmochim. Acta* **63,** 863–880.

Pokrovsky O. S. and Schott J. (2002) Surface chemistry and dissolution kinetics of divalent metal carbonates. *Environ. Sci. Tech.* **36,** 426–432.

Sangwal K. (1987) *Etching of Crystals: Theory, Experiment, and Application.* Elsever.

Schott J., Brantley S., Crerar D., Guy C., Borcsik M., and Willaime C. (1989) Dissolution kinetics of strained calcite. *Geochim. Cosmochim. Acta* **53,** 373–382.

Shiraki R., Rock P. A., and Casey W. H. (2000) Dissolution kinetics of calcite in 0.1 M NaCl solution at room temperature: An atomic force microscopic (AFM) study. *Aquat. Geochem.* **6,** 87–108.

Sjöberg E. L. and Rickard D. T. (1984a) Calcite dissolution kinetics: Surface speciation and the origin of the variable pH dependence. *Chem. Geol.* **42,** 119–136.

Sjöberg E. L. and Rickard D. T. (1984b) Temperature dependence of calcite dissolution kinetics between 1 and 62°C at pH 2.7 to 8.4 in aqueous solutions. *Geochim. Cosmochim. Acta* **48,** 485–493.

Stipp S. L. S., Eggleston C. M., and Nielsen B. S. (1994) Calcite surface structure observed at microtopographic and molecular scales with atomic force microscopy (AFM). *Geochim. Cosmochim. Acta* **58,** 3023–3033.

Teng H. H., Dove P. M., Orme C. A., and DeYoreo J. J. (1998) Thermodynamics of calcite growth: Baseline for understanding biomineral formation. *Science* **282,** 724–727.

Teng H. H., Dove P. M., and DeYoreo J. J. (2000) Kinetics of calcite growth: Surface processes and relationships to macroscopic rate laws. *Geochim. Cosmochim. Acta* **64,** 2255–2266.

Van Cappellen P., Charlet L., Stumm W., and Wersin P. (1993) A surface complexation model of the carbonate mineral-aqueous solution interface. *Geochim. Cosmochim. Acta* **57,** 3505–3518.

White A. F. Peterson M. L. (1990) Role of reactive-surface-area characterization in geochemical kinetic models. In *ACS Symposium Series: Chemical Modeling of Aqueous Systems II,* Vol. 416 (eds. D. C. Melchior and R. L. Bassett), pp. 461–475.

Yau S.-T., Thomas B. R., and Vekilov P. G. (2000) Molecular mechanisms of crystallization and defect formation. *Phys. Rev. Lett.* **85,** 353–356.